THE JOURNAL OF PHYSICAL CHEMISTRY C

Article

pubs.acs.org/JPCC

Study of the Partial Ag-to-Zn Cation Exchange in $AgInS_2$/ZnS Nanocrystals

Baodong Mao,[†] Chi-Hung Chuang,[†] Feng Lu,[†,‡] Lixia Sang,*[,†,§] Junjie Zhu,*[,‡] and Clemens Burda*[,†]

[†]Center for Chemical Dynamics and Nanomaterials Research, Department of Chemistry, Case Western Reserve University, 10900 Euclid Avenue, Cleveland, Ohio 44106, United States

[‡]State Key Laboratory of Analytical Chemistry for Life Science, School of Chemistry and Chemical Engineering, Nanjing University, Nanjing 210093, P. R. China

[§]Key Laboratory of Enhanced Heat Transfer and Energy Conservation, Ministry of Education and Key Laboratory of Heat Transfer and Energy Conversion, Beijing Municipality, Beijing University of Technology, Beijing, 100124, P. R. China

Supporting Information

ABSTRACT: $AgInS_2$–ZnS (AIZS) nanocrystals (NCs) were synthesized using a simple one-step approach by heating a Ag/In/Zn/S solution to 210 °C providing highly tunable photoluminescence (PL). The incorporation of Zn even at low temperatures (~150 °C) and the increased cation exchange of silver by zinc at higher temperatures strongly influence the optical properties of the resulting NCs. The correlation between synthesis parameters and resulting optical properties provided insights on the growth and stability of ternary and quaternary semiconductors. Systematic investigation with time-resolved spectroscopy showed distinguishable PL behaviors between developing and fully grown AIZS NCs. Attempts to coat as-prepared $AgInS_2$ NCs resulted in the same PL behavior as the one-step reaction product indicating that Zn readily exchanges with Ag ions even when not directly incorporated in the initial reaction mixture. Even with a low amount of zinc, the fully grown AIZS NCs showed improved PL QYs and single exponential decay behavior with long PL lifetimes. Control of the optical properties of these NCs makes them potentially useful for applications in photovoltaics and bioimaging particularly in light of their nontoxicity.

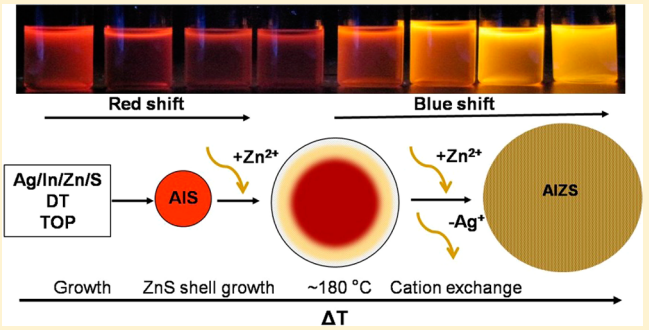

1. INTRODUCTION

Ternary I–III–VI semiconductors are direct band gap materials with high extinction coefficients in the visible to near-infrared region enabling a wide range of applications[1−4] such as printable solar cells[5,6] and bioimaging as an alternative for cadmium containing quantum dots (QDs).[7,8] The identified advantages of I–III–VI QDs, such as long PL lifetime and low toxicity, are important for bioimaging via controlling imaging acquisition time.[9,10]

Silver–indium-disulfide (AIS) based materials have a different chemistry from other I–III–VI materials because of the high reactivity of silver ions with sulfur even at low temperatures. Several methods based on thermolysis of various metal–sulfur complexes[11−14] or direct reaction of metal cations and sulfur[13,15−17] have been used to synthesize ternary AIS nanocrystals (NCs) with adjustable sizes by controlling capping reagents and reaction temperature and time. Donor–acceptor pair transitions at energies lower than the band gap have consistently been observed for the AIS NCs with corresponding broad emission peaks and relatively large Stokes shift due to the different kinds of defects such as sulfur and silver vacancies and interstitial atoms.[13,15,18] In our previous work, the effect of surface and intrinsic trap states on the optical properties of AIS NCs was investigated using time-resolved spectroscopy.[15] ZnS, a wide band gap semiconductor, is commonly used to improve the PL efficiency of semiconductor NCs through the elimination of surface trap states. Up to 10-fold improvement of the quantum yield was reported for ZnS coated $CuInS_2$NCs.[19] However, there are much fewer reports of ZnS coated AIS NCs in the literature.[15,20] Alternatively, ZnS-$AgInS_2$ solid solution nanoparticles were reported as a color-adjustable luminophores, in which the PL of the nanoparticles synthesized from a single precursor method can be tuned by the amount of Zn in the metal diethyldithiocarbamate precursor.[11] Recently, Tang et al. reported $AgInS_2$–ZnS heterodimers with tunable photoluminescence, which was achieved by controlling the diffusion of Zn ions into $AgInS_2$.[21,22] Zinc cation exchange[20,23] was also employed for synthesizing $CuInS_2$/ZnS and $AgInS_2$/ZnS core/shell NCs. The amount of Zn was directly related to the PL blue shift of all of the $AgInS_2$–ZnS NCs mentioned above. Moreover, several works were performed to study the PL enhancement or quenching of $AgInS_2$–ZnS NCs in

Received: September 16, 2012
Revised: November 29, 2012
Published: December 24, 2012

different environments.[24−27] These alloyed or core/shell $AgInS_2$−ZnS NCs show promise for applications in chemosensors[25] and bioimaging[21,27−29] fields.

With the rapid growth of research on semiconductor NCs, synthesis strategies such as alloying, doping, and strain-tuning have attracted much attention with regard to band gap and electronic wave function engineering.[30−36]In semiconductor heterostructures, alloying of the interfacial layer can reduce the lattice mismatch between the core/shell layers, where the graded or mixed compositions allow for gradual strain release with improved optical properties.[35,37,38] Nonblinking semiconductor NCs were reported using the radially graded alloy structure, which is of interest in applications requiring a continuous output of photons.[39]Another interesting phenomenon, due to the lattice strain effect, is that a type I heterostructure can be converted to a type II in (CdTe)ZnSe QDs through altering the energy band offsets of the two components.[30] The $AgInS_2$−ZnS system provides a good research model for multicomponent semiconductor NCs, in which $AgInS_2$ forms at very low temperature of ∼90 °C[15,16,21] and ZnS forms at higher temperature of ∼210 °C. The reaction chemistry of the $AgInS_2$−ZnS system is complicated and very intriguing. It can favor the design of NCs with widely tunable properties. However, it is still not well understood how to control the structure of the $AgInS_2$−ZnS NCs, to identify and distinguish experimentally the core/shell from an alloyed NC, and to tune the photophysical properties of these quaternary semiconductors as well as to demonstrate their PL mechanism.[20,21,26]Time-resolved spectroscopies[15,18,19,40] play a key role in better understanding the alloying and doping processes as well as in further optimization.

A series of $AgInS_2$−ZnS (denoted as AIZS) NCs was synthesized from a one-pot reaction by heating the Ag/In/Zn/S solution to 210 °C and extracting the NCs during the heating process. Notably, although the PL of the NCs showed a pronounced red shift initially, a blue-shifted PL was observed later with increasing reaction time and temperature. To the best of our knowledge, this behavior has not been reported in other ternary or quaternary NCs before.

Here, time-resolved PL spectroscopy was used to investigate the PL behavior of the AIZS NCs. The effect of the formation temperature and Ag/In/Zn ratio on the optical properties of the NCs is presented based on both steady state and time-resolved spectroscopy. This investigation provides insights into the growth of multicomponent semiconductor NCs and furthermore provides rational design criteria for quaternary semiconductor NCs.

2. EXPERIMENTAL SECTION

2.1. Chemicals. Indium acetylacetonate ($In(acac)_3$, 99%), silver nitrate ($AgNO_3$,99.5%), zinc stearate (99.5%), sulfur (99.5%), dodecanethiol (DT, 99%), trioctylphosphine (TOP, 90%), oleic acid (OA, 90%), and octadecene (ODE, 90%) were purchased from Sigma-Aldrich. Toluene (99.5%) and ethanol (anhydrous) were purchased from Fischer Scientific. All chemicals were used without further purification.

2.2. Synthesis of AIZS NCs. For synthesizing AIZS NCs from one-pot reaction, 0.2 mmol of $AgNO_3$, 0.2 mmol of $In(acac)_3$, 0.2 mmol of zinc stearate, 1 mmol of oleic acid, and 10 mL of ODE were heated up to 60 °C and kept at this temperature for 20 min in a 25 mL flask under Ar flow to remove oxygen. Subsequently, 2 mmol of DT was injected and the solution was heated up to 90 °C. After a clear solution of the metal precursors was obtained, a small amount of TOP (∼0.1 mL) was injected. Five minutes later, 0.6 mmol of sulfur dissolved in 6 mL of ODE was swiftly injected into the system. Then the system was heated to 210 °C at an average rate of ∼14 °C/min. A sharp drop of the temperature was observed after S injection and the temperature increase is slower at the beginning stage as shown in the insert in part a of Figure 1.

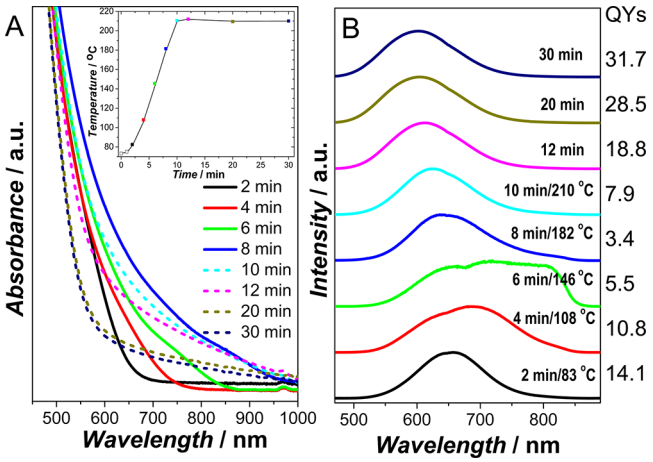

Figure 1. Normalized UV−vis absorption (a) and PL (b) spectra of the AIZS NCs synthesized from the one-pot reaction by heating the Ag/In/Zn/S precursor solution from 90 to 210 °C. For clarity, the PL spectra are vertically offset. Corresponding PL QYs (%) are shown at the right of panel (b). The insert in panel (a) shows the temperature increase over time.

Aliquots were extracted at different time intervals during the heating process and injected into equal amounts of cold toluene to get differently sized NCs. After synthesis, the NCs were washed with the toluene/ethanol cycles by centrifugation and then dissolved in toluene for storage.

To investigate the role of temperature, AIZS NCs were also synthesized by heating the same Ag/In/Zn/S solution from 120 °C, 150 °C, 180 °C, 210 to 230 °C and kept for 30 min for each step to ensure the full growth of the NCs at a desired temperature. For ZnS diffusion in presynthesized AIS NCs (denoted as AIS-Zn), the procedure is similar to that of the AIZS NCs studied but with a different injection sequence. Sulfur was injected into the Ag/In solution without Zn and kept at 120 °C for 20 min to obtain the AIS NCs. Zinc stearate in ODE was injected later and then the system was heated to 210 °C at the same rate as in the one-pot reaction. AIS NCs were synthesized as well from the one-pot reaction by heating the Ag/In/S solution with all synthesis parameters being the same as for the AIZS NCs. The only difference was the absence of zinc.

2.3. Characterizations. UV−vis absorption spectra were recorded using a Varian Cary 50 spectrometer and PL spectra were recorded using a Horiba Fluorolog 3 Spectrofluorometer with excitation at 450 nm. Fluorescence QYs of the NCs were calculated using Cresyl violet as the standard. The size and morphology of the AIZS NCs were characterized with a transmission electron microscope (TEM, JEOL 1200CX) at an accelerating voltage of 80 kV. Phase of the NCs was examined using a Scintag X-1 Advanced X-ray powder diffractometer (XRD) with Cu Kα radiation. Composition of the NCs was measured by atomic absorption spectroscopy (AAS, Varian SpectraAA 220 FS). The AIZS NCs were dissolved in

dx.doi.org/10.1021/jp309202g | J. Phys. Chem. C 2013, 117, 648−656

Table 1. Summary of Reaction Time, Temperature, Atomic Ratios of Ag:In:Zn from AAS, Particle Sizes from TEM, PL Peak Positions, Quantum Yields (QYs), and Deconvoluted PL Peaks for the AIZS NCs[a]

						deconvoluted PL peaks		
AIZS[b]	T/°C	Ag:In:Zn/%	size/nm	PL/nm	QYs/%	Peak1	Peak2	ratio[c]
2 min	83	47: 37: 16		657	14.1	653	777	27:1
6 min	146	45: 35: 21	1.9	719	5.5	644	745 (811[d])	0.94:1(:0.31)
8 min	182	46: 33: 21	2.7	636	3.4	635	701	1.48:1
10 min	210	37: 35: 28	3.0	624	7.9	614	663	1.18:1
30 min	210	18: 34: 48	3.3	602	31.7	579	630	0.66:1

[a]All values have <5% error. [b]Time of NC synthesis. [c]The ratio equals to Peak1/Peak2. [d]Peak3 in AIZS 6 min.

concentrated nitric acid and diluted to desired concentrations for AAS measurements. Time-resolved PL spectra were recorded with a Streak camera (Optronis) with excitation at 470 nm. The excitation pump pulse is tuned by an optical parametric amplifier (OPA, TOPAS, Lightconversion) based on the 780 nm, 150 fs pulses generated from a regenerative amplifier using a Clark MXR CPA 2001 fs laser system.

3. RESULTS AND DISCUSSION

3.1. Synthesis of AIZS NCs. Figure 1 shows the UV−vis absorption and PL spectra of the AIZS NCs extracted from the one-pot reaction. With increasing reaction time, the absorption showed continuous red shift at the beginning stages (2−8 min) as shown in the early spectra in part a of Figure 1. This is due to the decreased quantum size effect with increasing size, similar to many other semiconductor NCs. The temperature reaches 210 °C just before 10 min heating and after that the absorption spectra started to blue shift (AIZS 10−30 min), which cannot be explained with quantum size effects and indicates that ZnS started to play a role in the optical properties of the NCs. The absorption spectra further evolved with a continuous blue shift upon keeping the temperature at 210 °C for longer durations. The optical band gap of the AIZS NCs was estimated from the plot of $(\alpha h\nu)^2$ versus $h\nu$ (Figure S1 of the Supporting Information), where α is the absorbance and $h\nu$ is the energy. The band gap decreased from 2.18 eV (2 min) to 1.92 (6 min) and 1.82 eV (10 min) at the early stages and then started to increase to 2.06 (12 min), 2.36 (20 min), and 2.33 eV (30 min) showing a consistent trend as shown in the absorption spectra in part a of Figure 1. Compared with the band gap of bulk $AgInS_2$ (1.87 eV) and ZnS (3.5 eV),[41] the later stage (10 to 30 min) increase of the band gap can be related to the alloying process of $AgInS_2$ with ZnS.

The PL spectra of the AIZS NCs also showed a red shift first and a blue shift at later stages of the synthesis as shown in part b of Figure 1. At lower temperature (2−6 min, 83−146 °C), the AIZS NCs showed a PL red shifting from 657 to 719 nm, which can be attributed to the size increase of the NCs. AIS NCs are the main product in this stage as AIS was reported to form at as low as 90 °C or even lower temperature[15,21] and ZnS forms at a much higher temperature. For the AIZS sample at 6 min, although it has a PL maximum at 719 nm, the PL spectra show a large red shift to wavelengths over 800 nm, which is beyond the detection range of our available spectrometer. The PL QYs also decreased along with this red shift and reached the lowest value at 8 min, 182 °C as shown in part b of Figure 1 and Table 1. Broad PL peaks and large stokes shift are usually observed in the ternary I−III−VI semiconductor NCs due to the characteristic donor−acceptor pair transition. The broad PL peaks have been ascribed to different kinds of defect states in the I−III−VI semiconductor NCs. Here, PL spectra of the AIZS NCs were deconvoluted and each spectrum could be well fit with two Gaussian functions except for AIZS 6 min as shown in Table 1 and Figure S2 of the Supporting Information. The peak on the spectrally blue side (left) is labeled as Peak1 and the other one (right) is Peak2. The relative ratio changes with the reaction progress, including NC growth and zinc influx. At the early stages, the PL red shift is related to the change of the ratio of Peak1/Peak2 similar to pure AIS NCs in our previous work. The dramatic change of the ratio at the early stage of NC growth can be ascribed to the amount variation of surface defect states depending on the particle size.[15] With increasing reaction time (6 min), besides the red shift of both peaks, an additional peak appears at over 800 nm indicating newly produced defect states. This is observed for the first time in the $AgInS_2$−ZnS studies and a clear assignment has not been achieved. A possible factor is the change of the defect states resulted from the adsorption or incorporation of Zn on the NC surface. In semiconductor heterostructures, this large red shift may be attributed to the formation of trap states resulted from the lattice mismatch between the surface layer and the core.[35] In our AIZS NCs, however, caution must be employed as distinguishing between different layers is difficult (below). With further increasing time, Peak3 (811 nm) observed in AIZS 6 min disappears in the later stage with more zinc incorporation into the NCs. However, the ratio of Peak1/Peak2 changes prominently after 8 min, from 1.48:1 (8 min), 1.18:1(10 min) to 0.66:1 (30 min) with both peaks blue shifting continuously. The PL blue shift in the later stage can be ascribed to the increased band gap due to zinc incorporation, similar to the reported $AgInS_2$−ZnS or $CuInS_2$−ZnS NCs.[11,20,23] Because of the complicated situation in the quaternary AIZS NCs, it is a more complex task to establish a model for the PL evolution. More detailed discussion will be addressed by correlation with time-resolved PL results.

Even at short times (6 min) the PL spectrum has already started to blue shift as indicated by the increase of short wavelength emission around 650 nm. It is indicative of trap states that the PL blue shift starts earlier (after 6 min) than the blue shift of the absorption spectra (after 10 min). With further increase of the reaction time and temperature, the PL spectra showed continued blue shift (λ_{PL} = 636 nm for AIZS 8 min, 624 nm for AIZS 10 min, and 613 nm for AIZS 12 min) as indicated by both the decrease of long wavelength emission and the increase of short wavelength emission. This can be ascribed to the incorporation of ZnS into the NCs consistent with previous reports on $AgInS_2$−ZnS and $CuInS_2$−ZnS NC syntheses.[20,21] For AIZS 20 and 30 min, the PL spectra did not show an obvious blue shift but the QYs further increased to 28.5% and 31.7%, which may be attributed to the growth and crystallinity improvement of the NCs.[26] A ZnS shell might form

dx.doi.org/10.1021/jp309202g | J. Phys. Chem. C 2013, 117, 648−656

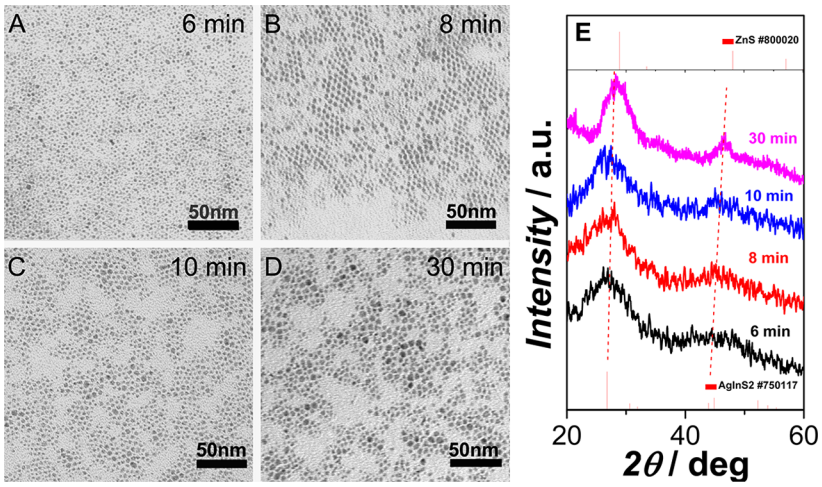

Figure 2. TEM images of the AIZS NCs synthesized at different times and temperatures: (a) 6 min, 1.9 ± 0.7 nm; (b) 8 min, 2.7 ± 0.7 nm; (c) 10 min, 3.0 ± 1.0 nm; (d) 30 min, 3.3 ± 1.2 nm; and (e) the corresponding XRD patterns.

on the AIZS NCs as indicated by the QY increase with no more blue shift after continuous heating at 210 °C. The temperature at 8 min, ~180 °C, may be a suggestive temperature for the formation of AIZS alloyed NCs to start.

TEM was used to demonstrate the size evolution with reaction time. Figure 2 shows the TEM images of the AIZS NCs extracted at different time intervals. The particles showed continuous size increase as expected. The sizes are 1.9 ± 0.7, 2.7 ± 0.7, 3.0 ± 1.0, and 3.3 ± 1.2 nm for AIZS 6, 8, 10, and 30 min, respectively. The increased size at higher temperature excludes the possibility that the absorption and PL blue shifts are due to NCs size decrease resulting from etching.

As shown in part e of Figure 2, XRD patterns of the AIZS NCs showed a medium phase of $AgInS_2$ and ZnS with the two main peaks (around 27° and 45°) positioned in middle of the standard patterns of bulk tetragonal AgInS2 (JCPDF #750117) and cubic ZnS (JCPDF 800020). With increasing time, the main peak shifts from 26.9° (AIZS 6 min) to 28.3° (AIZS 30 min) indicating the increasing amount of Zn, though the shift is not as obvious as previous reported $AgInS_2$–ZnS NCs.[11,21] However, because of the small sizes of the NCs, the XRD signal is relatively weak and the peaks are severely broadened, which makes the third peak (between 52.3° and 57.1°) usually observed in the $AgInS_2$–ZnS NCs difficult to identify. With increasing temperature, there is no obvious sign of phase change of the $AgInS_2$ NCs to orthogonal or cubic phases.

To examine the composition of the AIZS NCs, AAS was used to obtain accurate ratios of the different metal cations. The atomic ratios of Ag:In:Zn are 1.00: 0.78: 0.34, 1.00:0.96: 0.76, and 1.00: 1.84: 2.58 for AIZS 2, 10, and 30 min, respectively. This indicates the increasing Zn amount with increasing reaction time as well as particle growth. Even for AIZS 2 min at very low temperature (~83 °C), small amount of zinc has already been involved in the formation process. With increasing time, more zinc is incorporated into the NCs and a greater blue shift is observed, in agreement with a previous report.[21] However, the ratio of indium is constant in the range of 35 ± 2%, silver decreases from 47% to 18%, and zinc increases from 16% to 48% with increasing temperature. A plausible explanation is that zinc sulfide diffusion and cation exchange both occurred and, together, are responsible for the PL shifts in our AIZS NCs from the one-pot reaction. Additionally, this observation suggests that cation exchange of silver by zinc is preferential compared to that of indium, which is in contrast to the work by Tang et al.[21] After long reaction times, a ZnS shell might form on the AIZS NCs as indicated by the QY increase with no more blue shift after continuous heating at 210 °C.

3.2. Effect of Reaction Temperature. Although growth of the AIZS NCs was controlled by reaction time during synthesis, the reaction temperature is another critical parameter responsible for the structure and composition change as discussed above. The role of temperature on the formation of the AIZS NCs was further studied by keeping the system at low temperatures for longer time to allow the full growth of the particles at each step. As shown in part b of Figure 3, after heating at 120 and 150 °C for 30 min, there is no obvious PL blue shift, which indicates the absence of ZnS diffusion into AIS. However, there is an obvious blue shift after heating at 180 °C for 30 min. The PL maximum further shifted to 600 nm at 210 °C and stopped blue shifting upon heating at 230 °C but the QY increased as shown in part b of Figure 3. This is similar to the observation when heated at 210 °C from 12 to 30 min in the temperature ramping process (part b of Figure 1). The broad PL of the AIS NCs has been discussed earlier that was attributed to the deep donor–acceptor pair transitions.[13,15,18]

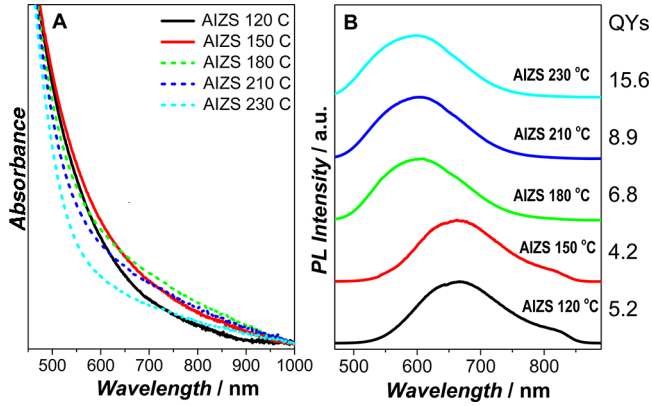

Figure 3. Normalized UV–vis absorption (a) and PL (b) spectra of the AIZS NCs synthesized by heating Ag/In/Zn/S from 120 to 230 °C. At the respective temperatures, the solutions were kept for 30 min to ensure the full growth of the NCs. For clarity, the PL spectra are vertically offset.

dx.doi.org/10.1021/jp309202g | J. Phys. Chem. C 2013, 117, 648–656

3.3. Zinc Diffusion into Preformed AIS NCs. A control experiment of Zn diffusion into AIS NCs was performed by injecting zinc stearate into presynthesized AIS NCs. The UV–vis absorption and PL spectra of the AIS and AIS-Zn NCs after zinc injection are shown in parts a and b of Figure 4,

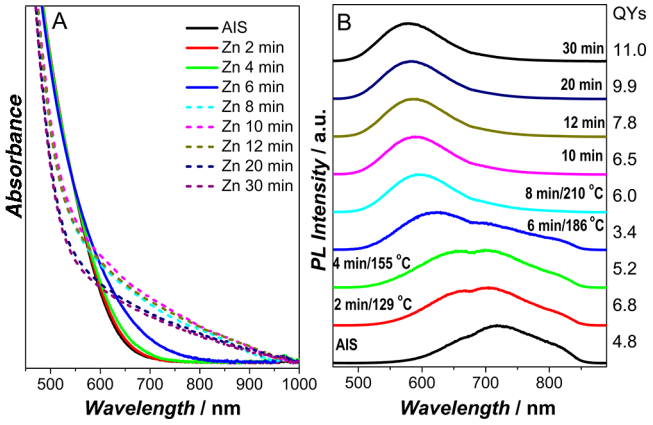

Figure 4. Normalized UV–vis absorption (a) and PL (b) spectra of the AIZS NCs synthesized by injecting zinc stearate/ODE into presynthesized AIS NCs and then increasing the temperature to 210 °C. For clarity, the PL spectra are vertically offset. The legend indicates the reaction time after zinc injection.

respectively. Sulfur was injected into the Ag/In solution and kept at 120 °C for 20 min to obtain the AIS NCs with λ_{PL} = 718 nm (part b of Figure 4). Subsequent zinc stearate injection and heating to 210 °C resulted in a continuous blue shift of the PL with increasing reaction time that is similar to the blue shift process of the Ag/In/Zn/S system (upper part of part b of Figure 1, 8 to 30 min). The PL QYs of the AIS-Zn NCs decreased with temperature increase and reached the lowest value (3.4%) at 6 min, 186 °C (part b of Figure 4), after which it started to increase, similar to the AIZS NCs in part b of Figure 1. This agrees well with our previous discussion that ZnS diffusion into AIS starts after ~180 °C. The reaction time, temperature, atomic ratios of Ag:In:Zn, PL peak positions, and QYs are shown in Table 2 for the AIS-Zn NCs. The

Table 2. Summary of Reaction Time, Temperature, Atomic Ratios of Ag:In:Zn, PL Peak Positions and QYs for the AIS-Zn NCs (Corresponding to the Samples Shown in Figure 4)[a]

AIS-Zn[b]	T/°C	Ag:In:Zn/%	PL/nm	QYs/%
2 min	129	43: 37: 19	706	6.8
6 min	186	45: 35: 19	621	3.4
8 min	210	42: 35: 23	593	6.0
10 min	210	43: 35: 22	591	6.5
30 min	210	26: 44: 30	579	11.0

[a]Values have <5% error. [b]Reaction time after zinc injection.

incorporation of zinc in the AIS-Zn NCs is not as efficient as that in the direction heating reaction of Ag/In/S/Zn solution. However, the similarities between the Ag/In/Zn/S and Ag/In/S+Zn systems, including PL shift, QYs variation and composition change, suggest that ZnS diffusion is responsible for the absorption and PL blue shift of the AIZS NCs similar to previous report.[21]

3.4. Synthesis of AIS NCs in Absence of Zinc. To better understand the role of zinc in the formation process, AIS NCs were also synthesized and investigated by heating the Ag/In/S solution to 210 °C for comparison. The precursor ratio of Ag:In:S was kept at 1:1:3 because stoichiometric ratio, e.g. Ag/In/S = 1:1:2, resulted in seriously aggregated particles at high temperature showing no PL. As shown in Figure 5, the red shift

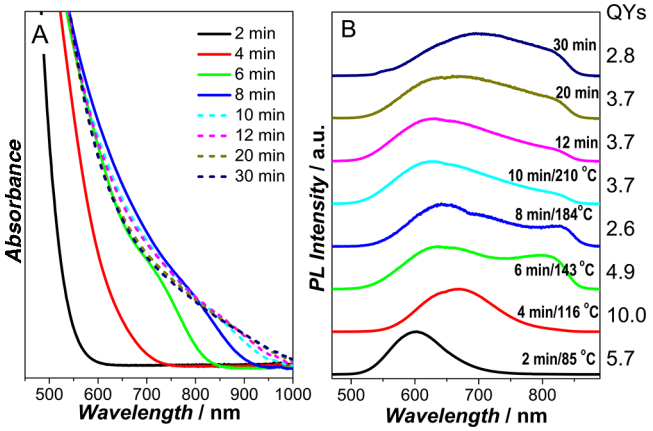

Figure 5. Normalized UV–vis absorption (a) and PL (b) spectra of the AIS NCs synthesized from the one-pot reaction by heating the Ag/In/S (1:1:3) solution from 90 to 210 °C. For clarity, the PL spectra are vertically offset.

of the absorption and PL spectra at the early stages was observed with the growth of the AIS NCs similar to AIZS NCs above. Compared with AIZS NCs, a difference is that the absorption shows almost no blue shift after 8 min upon long-time heating as shown in part a of Figure 5 (dashed curves). The elimination of long-wavelength PL was also not observed in direct contrast to AIZS NCs (part b of Figure 1). There is a dramatic change in PL from 4 to 6 min with temperature increase that has not been well understood. After 10 min, the long-wavelength PL increases gradually giving broad PL spectra with a fwhm of over 250 nm in all of the AIS NCs (10 to 30 min). Compared with λ_{PL} = 602 nm for AIZS 30 min, a broad PL peak with maximum at 700 nm for AIS 30 min suggests a different growing process of AIZS NCs and the integral role of zinc in the optoelectronic properties of AIZS materials.

3.5. Time-Resolved PL of the AIZS NCs. The I–III–VI semiconductor NCs are known for having donor–acceptor trap states and unique optical properties.[13,15,18,19] Alongside steady-state spectroscopy measurements, time-resolved spectroscopy was used to further characterize the emission properties of the AIZS NCs. Figure 6 shows the time-resolved PL spectra at different time delays after excitation. Time-resolved PL spectra of all the measured AIZS samples showed a red shift with increasing delay time. AIZS 6 min shows the largest red shift of over 30 nm with increasing delay time. The red-shifting emission indicates that PL decay rates are wavelength dependent, in which short-wavelength emission decays faster than long-wavelength emission. With the growth of the NCs, the red shift is less pronounced (parts b and c Figure 6, 8 and 10 min). This suggests that the different PL origins may vary with the growth of the NCs. The red shift was described as luminescence from trap state carrier recombination characteristic of ternary and quaternary semiconductors.[13,15,18] Compared with earlier studies on AIS NCs,[15,18] the PL red shift of the AIZS NCs with increasing delay time is less drastic. One

dx.doi.org/10.1021/jp309202g | J. Phys. Chem. C 2013, 117, 648–656

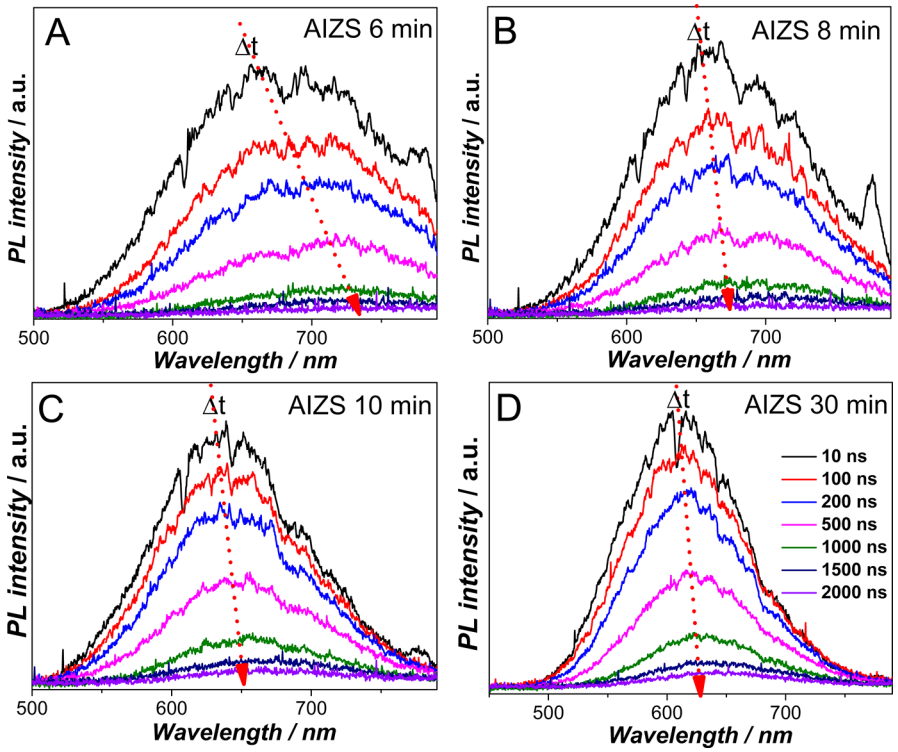

Figure 6. Time-resolved PL spectra of AIZS NCs synthesized by the one-pot reaction at different reaction times: (a) 6 min, (b) 8 min, (c) 10 min, and (d) 30 min. The legend in panel (d) shows the delay time after excitation. Red-shifting trend of the emission with increasing delay time is indicated by the dashed arrows.

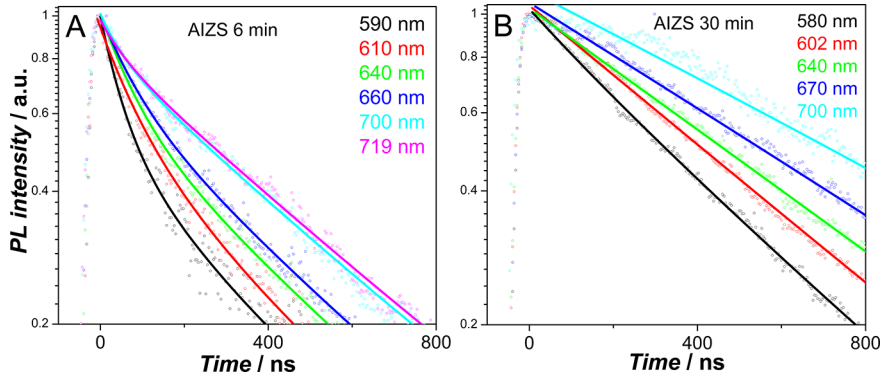

Figure 7. PL intensity decay curves of AIZS 6 min (a) and AIZS 30 min (b) NCs and the corresponding biexponential fitting curves. Colors of the legends correspond to the measured PL decay curves (circles) and the fitting curves (solid lines). Time constants are summarized in Table S1 of the Supporting Information.

plausible explanation is that the surface defect states are less prominent due to the existence of zinc during the growth process in the AIZS system.

Further analysis of the PL decay dynamics gives more insights into the optical properties and the growth process of the AIZS NCs. The PL decay curves were fit using biexponential functions with the data range of 3 μs to obtain lifetimes at different wavelengths, part of the data (800 ns) is shown here to give a magnified view of the results (Figure 7, AIZS 6 and 30 min). The fitting time constants for the samples (AIZS 2, 6, 8, 10, and 30 min) are summarized in Table S1 of the Supporting Information. At the PL maximum, AIZS 2 min, 6 and 8 min showed biexponential decay, whereas that of AIZS 10 and 30 min changed to single exponential decay.

As shown in part a of Figure 8, the average PL lifetimes of the AIZS NCs at different wavelength were obtained from biexponential fitting using $\tau_{ave} = (A_1\tau_1 + A_2\tau_2)/(A_1 + A_2)$. The averaged lifetimes at the PL maxima are 299, 438, 409, 558, and 552 ns for AIZS 2, 6, 8, 10, and 30 min, respectively. This indicates that the PL lifetime is size and composition dependent as well. There is a sharp increase of PL lifetime from AIZS 8 min to AIZS 10 min consistent with the observation of the beginning of the PL blue shift in the steady state spectra due to the diffusion of ZnS (Figure 1). For all of the smaller AIZS NCs synthesized at short time (2, 6, and 8 min), the ratio of the fast decay component $(A_1/(A_1 + A_2))$ decreased from ~50% to ~10% (part b of Figure 8) with increasing wavelength from 580 to 700 nm, which suggests that the fast decay component dominates at the short wavelength range and the slow decay component dominates at the long wavelength range of each PL spectrum similar to the observation for previously reported AIS NCs.[15]

dx.doi.org/10.1021/jp309202g | J. Phys. Chem. C 2013, 117, 648−656

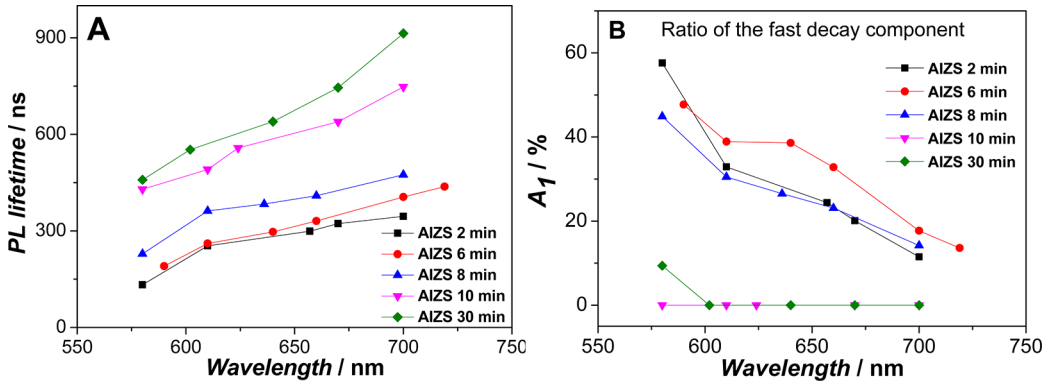

Figure 8. (a) Wavelength-dependent PL lifetimes of the AIZS NCs from the average of the biexponential fitting results using $\tau_{ave} = (A_1\tau_1 + A_2\tau_2)/(A_1 + A_2)$; (b) the ratio of the fast decay component $(A_1/(A_1 + A_2)$ in %) of the AIZS NCs. The related time constants are summarized in Table S1 of the Supporting Information.

The fast decay component is ascribed to surface defect states including vacancies and dangling bonds[15,18,19] providing local sites for relaxation of photoexcited electrons and holes resulting in fast decay rates compared to deep trap states. The decrease of the fast decay component with increasing reaction time indicates that surface passivation occurred during the growth of the AIZS NCs.[15] Most of the fast decay components have lifetimes falling into the range of 40−100 ns (Table S1 of the Supporting Information), comparable to previous reported values for ternary NCs in the absence of zinc that was assigned to surface defect states.[15,18,19] The slow decay component is ascribed to deep donor−acceptor pair transitions. In ternary semiconductors, the different kinds of intrinsic defects such as vacancies and interstitial atoms are well-known as deep trap states and responsible for the deep donor−acceptor pair transition.[13,15,18] No PL lifetime was reported in recent $AgInS_2-ZnS$ works.[11,20,21] Compared with $Zn_xCu_yInS_{1.5+x+0.5y}$ alloy NCs (τ_1 = 58−98 ns and τ_2 = 306−375 ns),[42] our AIZS NCs showed τ_1 in the same scale but much longer τ_2 (Table S1 of the Supporting Information).

Another important parameter is the decay rate of the exciton, both radiative and nonradiative. The radiative decay rate can be calculated by the equation $k_{rad} = QY/\tau_{fl} = 1/\tau_{rad}$, whereby QY is the quantum yield measured by steady state spectroscopy, τ_{fl} is PL lifetime measured by time-resolve PL spectroscopy, and τ_{rad} is the radiative decay lifetime. And then from the equation $k_{tot} = k_{nrad} + k_{rad} = 1/\tau_{fl}$, the nonradiative decay rate k_{nrad} can be calculated by the $k_{nrad} = 1/\tau_{fl} - 1/\tau_{rad}$ from τ_{rad} and τ_{fl}. The results are summarized in Table 3. A slow recombination rate suggests involvement of trap states. The radiative decay rate decreases from 2 min (4.72×10^5 s^{-1}) to 8 min (8.87×10^4 s^{-1}), which suggests that the density of trap states increases at the early growing stages of the AIZS NCs. After that, the radiative decay rate started to increase drastically (10 and 30 min). The nonradiative decay rates are 1 order of magnitude larger than the radiative decay rates for the early stage AIZS NCs (2 to 10 min) and showed a decreasing trend with increasing zinc incorporation from 2 to 30 min synthesis time. This is additional evidence for the elimination of defect states with the involvement of zinc.

Table 3. Summary of QYs, PL Lifetime (τ_{fl}), Radiative Decay Rate, and Nonradiative Decay Rate

AIZS	QYs/%	τ_{fl}[a]/ns	k_{rad}/s^{-1}	k_{nrad}/s^{-1}
2 min	14.1	299	4.72×10^5	2.87×10^6
6 min	5.5	437.8	1.26×10^5	2.16×10^6
8 min	3.4	383.2	8.87×10^4	2.52×10^6
10 min	7.9	557.6	1.42×10^5	1.65×10^6
30 min	31.7	552.3	5.74×10^5	1.24×10^6

[a]Average PL lifetime at the peak wavelength.

Based on the above results, the incorporation of ZnS resulted in two dramatic changes: (i) elimination of the fast decay component related to surface defects and ii) extension of the overall lifetime due to the transformation from AIS to AIZS. The first function of Zn can be attributed to the passivation of surface defects similar to that of ZnS coating[15,19] and the second one can be attributed to the change of the local environment[43] of the deep trap sites from AIS to AIZS that results in increased PL lifetimes. The incorporation of zinc resulted in a change of relative PL intensity ratio of the defect states that is related with PL peak position and also enhanced the PL QYs consistent with recent work on zinc cation exchanged I−III−VI NCs.[20,22,23] Part of our reaction process is more comparable to Torimoto's work, in which the effect of postsynthesis treatment on the AIS and $ZnS-AgInS_2$ NCs was explored and the absorption and PL shifts were ascribed to the change in the amount of defect sites inside the NCs with heat treatment.[26] In the early stage of AIS thin film studies, the intrinsic defects were investigated by annealing in different atmospheres and were mainly composed by silver (sulfur) vacancies and silver (sulfur) interstitials and their combinations. In Dai's recent work, PL enhancement of AIS NCs was investigated by changing the ratio of Ag^+ to total metal ions (Ag + In) and an optimized ratio of 0.37 was found, which was ascribed to the optimum amount of Ag vacancies as trapping sites for donor−acceptor pair recombination.[44] With more profound studies ongoing, more evidence pointed to the fact that the PL of the ternary semiconductor NCs can be tuned by the amount of the defect states,[13,15,18] among which group IB element (Cu or Ag) vacancies played a key role.[23,44] As observed in our results, complete ZnS shell coating is not necessary for large PL enhancement, which further supports the concept of defect state tuning by partial cation exchange in the presented AIZS NCs. The fully grown AIZS NCs showed extremely long PL lifetimes and single exponential decays indicating the superior optical and structural properties even with a small amount of zinc (Ag/In/Zn = 1.00: 0.96: 0.76 for AIZS 10 min).

dx.doi.org/10.1021/jp309202g | J. Phys. Chem. C 2013, 117, 648−656

4. CONCLUSIONS

In summary, a series of AIZS NCs was synthesized from a one-step reaction by heating the Ag/In/Zn/S precursor solution to 210 °C and studying the extracted NCs with steady-state and time-resolved optical spectroscopies. The AIZS NCs are distinctly different from other I−III−VI NCs because of the high reactivity of the silver cation with sulfur at low temperatures <90 °C. Notably, the PL of the NCs showed pronounced wavelength dependence with zinc addition, reaction time, and temperature increase. To the best of our knowledge, the observed PL behavior has not been systematically documented in any other ternary or quaternary NCs before. Monitoring the PL of the NCs during the temperature rise allowed us to study the optical properties during the alloying and Ag-to-Zn cation exchange process. As a comparative control, additional series of experiments were performed to investigate the effect of temperature and growth alone, as well as additional zinc addition to $AgInS_2$ NCs. The transformation to AIZS started at ∼180 °C but was not complete until 210 °C as indicated by a sharp increase in the PL QYs and lifetimes. A preferred cation exchange of silver ions by zinc was observed compared to the relatively constant indium content in the NCs as studied with AAS analysis. Systematic investigation of the PL decay dynamics shows how the electronic relaxation dynamics depends on size and composition controlled by reaction time and temperature. The fastest relaxation component, due to carrier trapping, could be eliminated during the growth process through passivation of the surface with a small amount of zinc ions. However, larger amounts of zinc addition at temperatures above 180 °C lead to cation exchange and significantly changed the optical properties. This investigation provides insights into the growth of multicomponent semiconductor NCs and furthermore provides rational design criteria for quaternary semiconductor NCs. In view of their widely tunable PL in the visible to NIR range, AIZS NCs may have applications for future designs of nanostructured solar cells, photocatalysts, and bioimaging reagents.

■ ASSOCIATED CONTENT

Ⓢ Supporting Information

Estimation of band gaps, Gaussian deconvolution of the PL spectra, and biexponential fitting results of the PL decay curves of the AIZS NCs. This material is available free of charge via the Internet at http://pubs.acs.org.

■ AUTHOR INFORMATION

Corresponding Author

*E-mail: burda@case.edu; Phone: (216)368-5918; Fax: (216) 368-3006.

Notes

The authors declare no competing financial interest.

■ REFERENCES

(1) Shay, J. L.; Wernick, J. H. *Ternary Chalcopyrite Semiconductors: Growth, Electronic Properties, and Applications*; Pergamon Press, 1975.
(2) Klenk, R.; Klaer, J.; Scheer, R.; Lux-Steiner, M. C.; Luck, I.; Meyer, N.; Ruhle, U. *Thin Solid Films* **2005**, *480*, 509−514.
(3) Tsuji, I.; Kato, H.; Kudo, A. *Angew. Chem., Int. Ed.* **2005**, *44*, 3565−3568.
(4) Zhong, H.; Bai, Z.; Zou, B. *J. Phys. Chem. Lett.* **2012**, *3*, 3167−3175.
(5) Li, L.; Coates, N.; Moses, D. *J. Am. Chem. Soc.* **2010**, *132*, 22−23.
(6) Panthani, M. G.; Akhavan, V.; Goodfellow, B.; Schmidtke, J. P.; Dunn, L.; Dodabalapur, A.; Barbara, P. F.; Korgel, B. A. *J. Am. Chem. Soc.* **2008**, *130*, 16770−16777.
(7) Allen, P. M.; Bawendi, M. G. *J. Am. Chem. Soc.* **2008**, *130*, 9240−9241.
(8) Omata, T.; Nose, K.; Otsuka-Yao-Matsuo, S. *J. Appl. Phys.* **2009**, *105*, 073106.
(9) Li, L.; Daou, T. J.; Texier, I.; Tran, T. K. C.; Nguyen, Q. L.; Reiss, P. *Chem. Mater.* **2009**, *21*, 2422−2429.
(10) Wang, L. L.; Zheng, H. Z.; Long, Y. J.; Gao, M.; Hao, J. Y.; Du, J.; Mao, X. J.; Zhou, D. B. *J. Hazard. Mater.* **2010**, *177*, 1134−1137.
(11) Torimoto, T.; Adachi, T.; Okazaki, K.; Sakuraoka, M.; Shibayama, T.; Ohtani, B.; Kudo, A.; Kuwabata, S. *J. Am. Chem. Soc.* **2007**, *129*, 12388−12389.
(12) Feng, Z. Y.; Dai, P. C.; Ma, X. C.; Zhan, J. H.; Lin, Z. J. *Appl. Phys. Lett.* **2010**, *96*, 013104.
(13) Ogawa, T.; Kuzuya, T.; Hamanaka, Y.; Sumiyama, K. *J. Mater. Chem.* **2010**, *20*, 2226−2231.
(14) Du, W. M.; Qian, X. F.; Yin, J.; Gong, Q. *Chem.—Eur. J.* **2007**, *13*, 8840−8846.
(15) Mao, B.; Chuang, C.-H.; Wang, J.; Burda, C. *J. Phys. Chem. C* **2011**, *115*, 8945−8954.
(16) Xie, R. G.; Rutherford, M.; Peng, X. G. *J. Am. Chem. Soc.* **2009**, *131*, 5691−5697.
(17) Wang, D. S.; Zheng, W.; Hao, C. H.; Peng, Q.; Li, Y. D. *Chem. Commun.* **2008**, 2556−2558.
(18) Hamanaka, Y.; Ogawa, T.; Tsuzuki, M.; Kuzuya, T. *J. Phys. Chem. C* **2011**, *115*, 1786−1792.
(19) Li, L.; Pandey, A.; Werder, D. J.; Khanal, B. P.; Pietryga, J. M.; Klimov, V. I. *J. Am. Chem. Soc.* **2011**, *133*, 1176−1179.
(20) Park, J.; Kim, S. W. *J. Mater. Chem.* **2011**, *21*, 3745−3750.
(21) Tang, X.; Yu, K.; Xu, Q.; Choo, E. S. G.; Goh, G. K. L.; Xue, J. *J. Mater. Chem.* **2011**, *21*, 11239−11243.
(22) Tang, X.; Ho, W. B. A.; Xue, J. M. *J. Phys. Chem. C* **2012**, *116*, 9769−9773.
(23) De Trizio, L.; Prato, M.; Genovese, A.; Casu, A.; Povia, M.; Simonutti, R.; Alcocer, M. J. P.; D'Andrea, C.; Tassone, F.; Manna, L. *Chem. Mater.* **2012**, *24*, 2400−2406.
(24) Kameyama, T.; Okazaki, K. I.; Ichikawa, Y.; Kudo, A.; Kuwabata, S.; Torimoto, T. *Chem. Lett.* **2008**, *37*, 700−701.
(25) Uematsu, T.; Taniguchi, S.; Torimoto, T.; Kuwabata, S. *Chem. Commun.* **2009**, 7485−7487.
(26) Torimoto, T.; Ogawa, S.; Adachi, T.; Kameyama, T.; Okazaki, K. I.; Shibayama, T.; Kudo, A.; Kuwabata, S. *Chem. Commun.* **2010**, *46*, 2082−2084.
(27) Chang, J.-Y.; Wang, G.-Q.; Cheng, C.-Y.; Lin, W.-X.; Hsu, J.-C. *J. Mater. Chem.* **2012**, *22*, 10609−10618.
(28) Koktysh, D.; Bright, V.; Pham, W. *Nanotechnology* **2011**, *22*, 275606.
(29) Sheng, Y.; Tang, X.; Xue, J. *J. Mater. Chem.* **2011**, *22*, 1290−1296.
(30) Smith, A. M.; Nie, S. M. *Acc. Chem. Res.* **2010**, *43*, 190−200.
(31) Zhong, X.; Feng, Y.; Knoll, W.; Han, M. *J. Am. Chem. Soc.* **2003**, *125*, 13559−13563.
(32) Erwin, S. C.; Zu, L. J.; Haftel, M. I.; Efros, A. L.; Kennedy, T. A.; Norris, D. J. *Nature* **2005**, *436*, 91−94.
(33) Bailey, R. E.; Nie, S. M. *J. Am. Chem. Soc.* **2003**, *125*, 7100−7106.
(34) Mocatta, D.; Cohen, G.; Schattner, J.; Millo, O.; Rabani, E.; Banin, U. *Science* **2011**, *332*, 77−81.
(35) Lo, S. S.; Mirkovic, T.; Chuang, C. H.; Burda, C.; Scholes, G. D. *Adv. Mater.* **2011**, *23*, 180−197.
(36) Chen, X. B.; Lou, Y. B.; Samia, A. C.; Burda, C. *Nano Lett.* **2003**, *3*, 799−803.
(37) Manna, L.; Scher, E. C.; Li, L.-S.; Alivisatos, A. P. *J. Am. Chem. Soc.* **2002**, *124*, 7136−7145.
(38) Ivanov, S. A.; Piryatinski, A.; Nanda, J.; Tretiak, S.; Zavadil, K. R.; Wallace, W. O.; Werder, D.; Klimov, V. I. *J. Am. Chem. Soc.* **2007**, *129*, 11708−11719.

(39) Wang, X. Y.; Ren, X. F.; Kahen, K.; Hahn, M. A.; Rajeswaran, M.; Maccagnano-Zacher, S.; Silcox, J.; Cragg, G. E.; Efros, A. L.; Krauss, T. D. *Nature* **2009**, *459*, 686−689.
(40) Chuang, C. H.; Burda, C. *J. Phys. Chem. Lett.* **2012**, *3*, 1921−1927.
(41) Shay, J. L.; Tell, B.; Schiavon, Lm; Kasper, H. M.; Thiel, F. *Phys. Rev. B* **1974**, *9*, 1719−1723.
(42) Feng, J.; Sun, M.; Yang, F.; Yang, X. R. *Chem. Commun.* **2011**, *47*, 6422−6424.
(43) Tang, X. S.; Cheng, W. L.; Choo, E. S. G.; Xue, J. M. *Chem. Commun.* **2011**, *47*, 5217−5219.
(44) Dai, M. L.; Ogawa, S.; Kameyama, T.; Okazaki, K.; Kudo, A.; Kuwabata, S.; Tsuboi, Y.; Torimoto, T. *J. Mater. Chem.* **2012**, *22*, 12851−12858.